Finite Element Deformation Analysis
of Fuel Cell Metal Bipolar Plate with Distorted Design Features

Shou-I Chen,[1*] Ming-Lung Li,[2] Yu-Lin Song,[3] Yu-Hsu Chen,[4] and Wei-Jen Chen[5**]

[1]Department of Mechanical Design Engineering, National Formosa University, Yunlin 63201, Taiwan
[2]National Center for High-Performance Computing, National Applied Research Laboratories,
Hsinchu 30076, Taiwan
[3]Department of Bioinformatics and Medical Engineering, Asia University, Taichung City 41170, Taiwan
[4]College of Medicine, Taipei Medical University, Taipei City 110301, Taiwan
[5]Department of Aeronautical Engineering, Chaoyang University of Technology, Taichung City 41170, Taiwan

The assembly locking compression force of the fuel cell directly impacts the contact area between the metallic bipolar plate (MBP) and the membrane electrode assembly (MEA), thereby affecting the electrical resistance of the fuel cell stack. In this study, we employed the finite element method to build a fuel cell stack simulation model to analyze the deformation and warpage of the MBP after being subjected to locking force. Through nonlinear contact elements, we showed the contact area and pressure distribution between the MBP and the MEA. The research results indicated that, owing to the effects of bolt locking, the left and right sides of the interface between the MBP and the MEA are the main contact areas transmitting the contact pressure. This area forms the primary support points for the bending load, leading to upward or downward warping deformation, and causes noticeable gaps between the bipolar plates and the MEA. In addition, distorted design features were added to the MBP to compare and improve the deformation of the MBP. The results showed that the bipolar plate with distorted design features can effectively reduce the maximum vertical deformation by 10.3%, which will effectively improve the contact area between the bipolar plate and the MEA module. This will effectively reduce the contact resistance of the fuel cell.

1. Introduction

Fuel cells have broad application prospects in energy harvesting. By integrating fuel cells with various energy harvesting technologies, it is possible to improve efficient energy conversion and utilization. This integration provides stable and reliable power, supporting a wide range of applications from portable devices to large-scale infrastructure. A proton exchange membrane fuel cell (PEMFC) primarily consists of a membrane electrode assembly (MEA) and a metal bipolar plate (MBP), forming a sandwich-like structure. It is clamped together under pressure by the bolts of the end plates. Accurate assembly is crucial to prevent leaks, establish a uniform

---

distribution of contact pressure, and reduce contact resistance.[1] Increasing the bolt tightening force and the number and location of bolts reduces the internal contact resistance of the fuel cell. Excess compression can also cause fuel cell components to experience excessive mechanical stress, leading to issues such as rupture, gas leakage, and liquid leakage. Uneven compression during locking can result in either too high or too low volumetric flow rates of reactants, causing uneven current distribution and the formation of localized hotspots, accelerating the degradation of the MEA and the formation of pinholes. Excess contact pressure may lead to deformation and damage to the gas diffusion layer (GDL)[2,3] and MEA modules, thereby affecting the performance of the fuel cell.[4–10] Many previous studies have explored various combinations of bolt configurations and tightening torque[11,12] and used finite element analysis to investigate the effects of the number, location, and assembly parameters of MEA modules in fuel cell stacks on the MBP contact area. Most of the above-mentioned research goals focus on improving the compression uniformity of the contact area between the MBP and the MEA modules.[1,13,14]

In current standardized fuel cell stacks, the main approach involves achieving consistency in the assembled fuel cell stack through pressure control. However, while the bolt tightening force can be effectively managed during stack assembly, performance aspects such as the compatibility between the electrodes and the bipolar plates in the fuel cell cannot be adequately controlled.[1,15,16] Consequently, this leads to low yield in assembled products, often resulting in issues such as gas leakage, liquid leakage, or poor performance of individual cells, causing the failure of the entire fuel cell stack.[16–18]

The preliminary research results indicate that appropriately designed distortion features in the MBP can effectively reduce contact impedance, preventing the continuous increase in bolt tightening pressure during assembly to maintain contact impedance.[19,20] This approach minimizes the differences among fuel cell units, thus avoiding other complex designs to increase the compressive force. In this study, we employed finite element simulation analysis to establish a suitable model for a fuel cell stack. The purpose is to understand the deformation of the MBP under the pressure of bolt locking in the fuel cell stack model. In this study, we will validate the analysis results by comparing with previous literature[21] and further explore the effects of distortion features on MBP deformation, providing recommendations for future design improvements.[22–24]

2. Materials and Methods

In order to compare with the experimental results of previous studies exploring the distorted design features of the MBP, we constructed a finite element model of the fuel cell stack based on the components used in this research.[21] The composition and parts of the fuel cell stack model in this study are shown in Fig. 1. In the figure, the green components represent the MEA modules, the blue and red components represent two different materials of gaskets, the gray components are the bipolar plates, and the yellow components are the top and bottom end plates. Each single cell consists of the MEA, the MBP, and two types of gasket. The fuel cell stack model studied in this research comprises eight sets of single cell assemblies, and the top and bottom end plates form the entire fuel cell stack.[22,23,25]
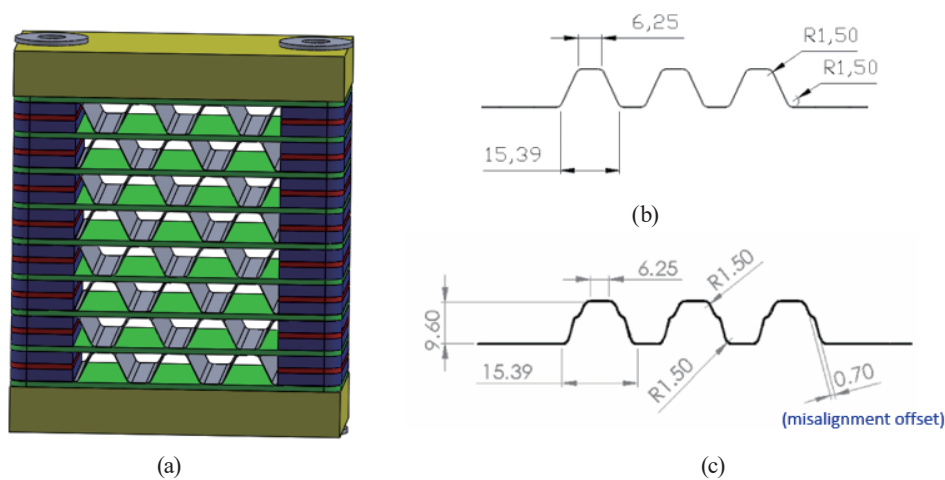
Fig. 1. (Color online) Model of fuel cell stack and two different flow channel features of MBP.[21] (a) Fuel cell stack Model, (b) normal MBP, and (c) MBP with distorted feature.

For the normal trapezoidal MBP with flow channel features, detailed geometric dimensions are shown in Fig. 1(b). In this study, a distorted design feature was implemented on the MBP, setting the misalignment offset on both sides to 0.3 and 0.7 mm. This was done to investigate the impact of this feature design on the warping of the MBP and to compare it with relevant research papers.

In this study, a 1/2 model symmetry setting is adopted for the constructed 3D finite element model of the fuel cell stack. The mesh setting for components such as the MEA, gasket, and end plate adopts a hexahedral mesh construction with an element size of 2.0 mm. However, owing to the irregular shape of the bipolar plate caused by the distorted design features, a tetrahedral mesh construction is employed with an element size of 1.5 mm. The entire fuel cell stack analysis model consists of a total of 327857 nodes, with a total of 113404 mesh elements.

The 3D fuel cell stack solid model was constructed using the computer-aided design software SolidWorks (SolidWorks 2016; Dassault Systems SolidWorks Corporation, Waltham, MA, USA). Subsequently, finite element simulation analysis was performed using the commercial code of ANSYS (ANSYS 19.0, ANSYS Inc., Canonsburg, PA, USA) to analyze deformations and the gap between the MBP and the MEA. In the finite element model, the material properties for the MEA, Gasket1, and end plate in this fuel cell model are set as steel, with a Young's modulus of 345 MPa and a Poisson's ratio of 0.3. The material properties for Gasket2 are set as rubber with a Young's modulus of 16 MPa and a Poisson's ratio of 0.45. The MBP is set as stainless steel with a Young's modulus of 206 MPa and a Poisson's ratio of 0.247.[6,15]

Under the boundary conditions, the analysis model explores the contact areas and the gaps generated between each layer of bipolar plates and MEA structures. Local gaps will increase the contact resistance, which affects the overall impedance of the fuel cell stack. Therefore, contact elements are employed to simulate the compression or separation of interfaces between the MEA module and the MBP, as shown in Fig. 2. In the analysis model, a load of 1.5 N is applied to the
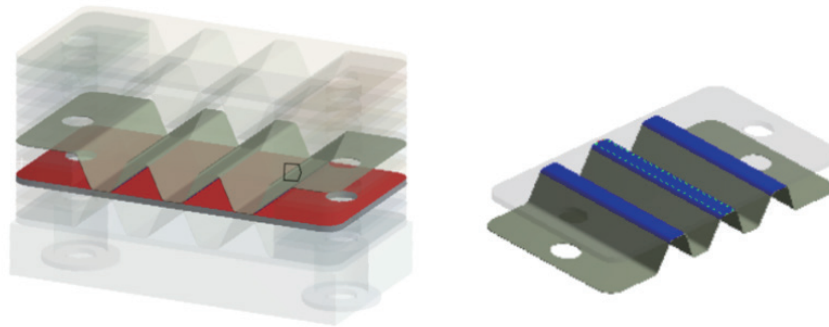
Fig. 2.   (Color online) Contact interface between MBP and MEA.

bolt region of the fuel cell base, and symmetric boundary conditions are set on the symmetry plane of the 1/2 model.

3.   Results

Figure 3 shows the overall deformation analysis results of the symmetrical fuel cell stack using finite element analysis. In Fig. 3(a), the entire fuel cell stack undergoes almost uniform downward deformation due to the tightening force of the bolts on the upper and lower end plates, with a deformation value of approximately 0.003 mm. The deformation values of the upper end plate and the left and right gaskets are similar, but the bipolar plate components exhibit more noticeable geometric deformations. In particular, there is a significant relative displacement observed in the middle region of the upper plane of the trapezoidal structure of the MBP and MEA, as depicted in Fig. 3(b).

In Fig. 3(c), the sectional plot of the trapezoidal structure of the MBP clearly reveals significant deformations and warping. The trapezoidal geometric structure of the bipolar plates undergoes noticeable deformations and warping. Owing to the relatively high material strength of the two end plate components and the gasket elements on two sides of the fuel cell stack, the overall results of the deformation analysis indicate predominant displacement in the vertical direction.

The vertical displacement (Y-direction) of the fuel cell stack model is shown in Fig. 4. In the figure, positive values represent upward displacement whereas negative values represent downward displacement. The results of the analysis indicate that the overall external structure of the fuel cell experiences nearly zero displacement in the vertical direction (depicted by the green region). It should be noted that each layer of bipolar plates, particularly in the region adjacent to the lower MEA, exhibits an upward warping displacement, with a maximum warping value of approximately 0.1085 mm.

Similarly, the MBP exhibits a downward warping displacement with a maximum value of 1.085 mm in the region adjacent to the upper MEA. In Fig. 4, the bipolar plates in the regions adjacent to the upper and lower MEAs are defined as A1, A2, A3, A4, and A5, respectively. The
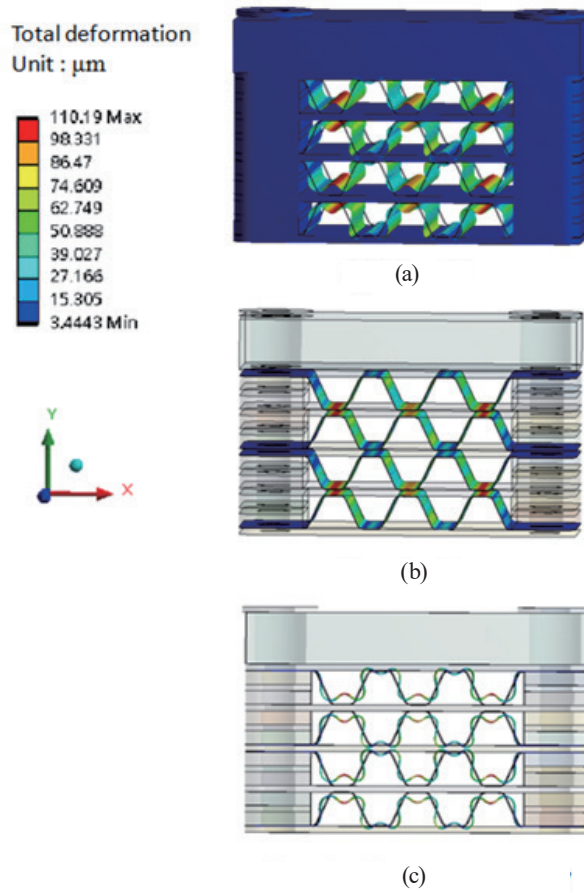
Fig. 3.　(Color online) Results of total deformation on fuel cell stack model. (a) Full model, (b) bipolar plate, and (c) bipolar plate cross-sectional view.
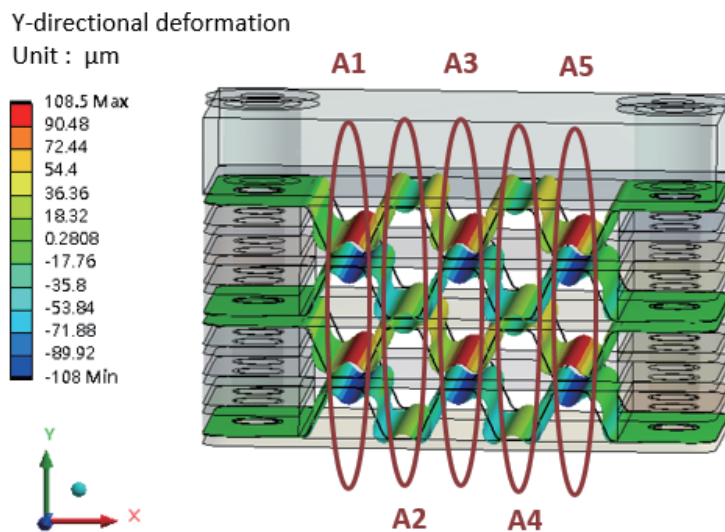

Fig. 4.　(Color online) Distribution results of Y-directional deformation on fuel cell stack model.

vertical displacement values of the trapezoidal bipolar plate structure in the A2 and A4 regions are smaller, indicating a smaller gap between the MBP and the MEA in these areas. This results in a larger electrode contact area and a reduced contact resistance.

Between the MBP and the MEA, this research analysis model uses contact elements to represent the pressure gap and contact area at the interface of the two. Figure 5 shows the distribution of the contact pressure for the contact elements between the interfaces. The analysis results showed that the contact area in the vicinity of the upper and lower MEAs in the bipolar plate structure is rectangular, as indicated by the blue region in the figure. On both sides of each rectangular contact area, there is a noticeable contact pressure from the squeezing contact between the MBP and the MEA. In Fig. 6, the results indicate that a microgap of approximately 30 µm is generated in the central region of the rectangular contact area between each bipolar
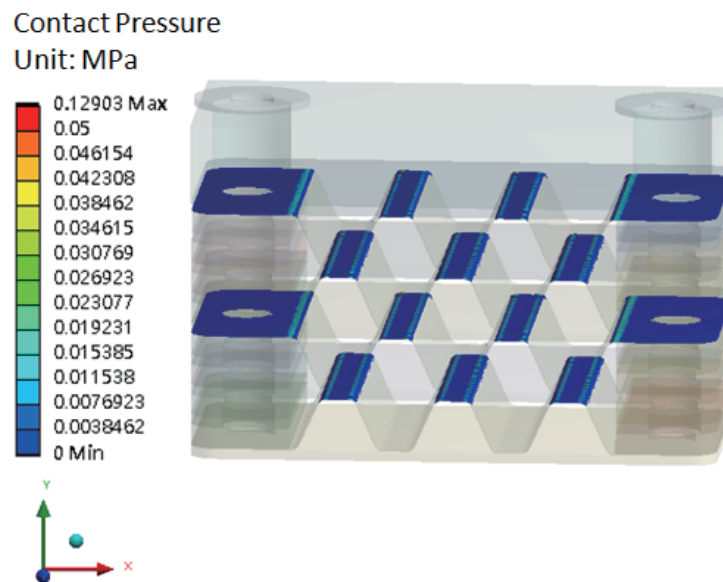

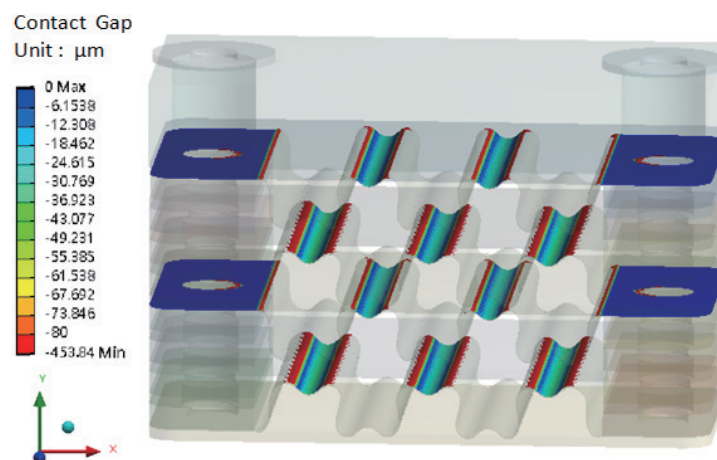Fig. 5.   (Color online) Contact pressure between MBP and MEA.

Fig. 6.   (Color online) Contact gap between MBP and MEA.

plate and the MEA. This gap will lead to an increase in contact resistance, resulting in a decrease in the efficiency of the cell reaction.

Regarding the results of the stress analysis, the regions with higher stress are primarily distributed on the MBP. As shown in Fig. 7, the maximum stress values occur at the corners of the trapezoidal structure and in the central area of the contact region between the MBP and the MEA module. This corresponds to the earlier observation of larger deflections in the bipolar plate.

By incorporating a distortion feature design[7] into the flow channel of the MBP, as shown in Fig. 1, we compared the different distortion feature designs with 0.3 and 0.7 mm offsets. The bar chart in Fig. 8 illustrates the comparison of their maximum vertical deformation values. The analysis results indicate that the MBP with a distorted design feature, with 0.3 mm offset, reduces the maximum displacement to 103.31 μm. Adopting a 0.7 mm distortion feature further decreases the maximum displacement to 98.978 μm. Compared with the 0.3- and 0.7-mm-offset MBPs, the maximum displacement of the normal MBP model is 108.52 μm, which is significantly reduced by 5.21 (4.8%) and 11.21 μm (10.3%), respectively. The results demonstrate that bipolar plates with a distortion feature design effectively reduce the maximum vertical displacement on the MBP, resulting in a reduction of 10.3%. Figure 9 shows that the 0.3- and 0.7-mm-offset MBPs with a distorted design feature has maximum vertical stress values of 0.36
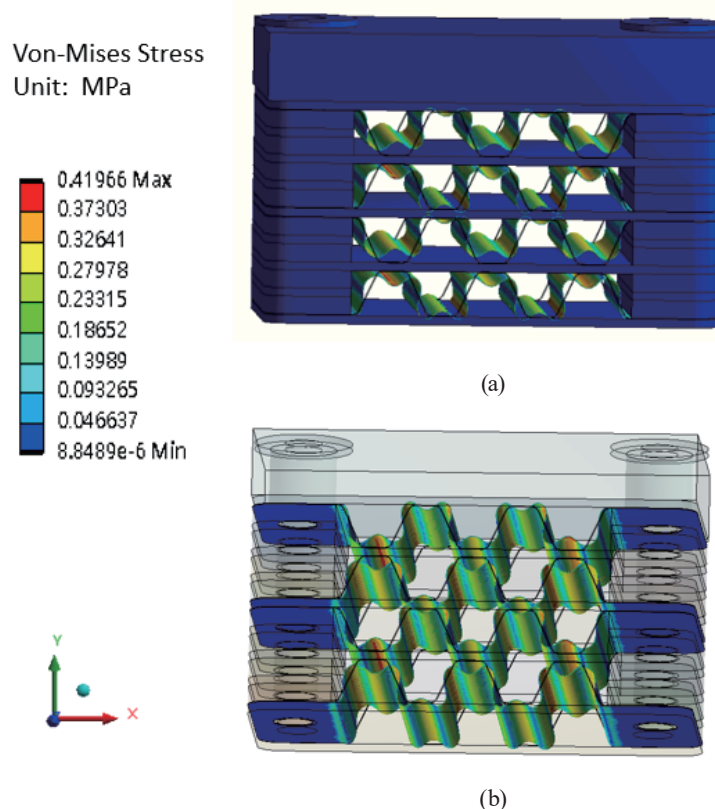

(a)

(b)

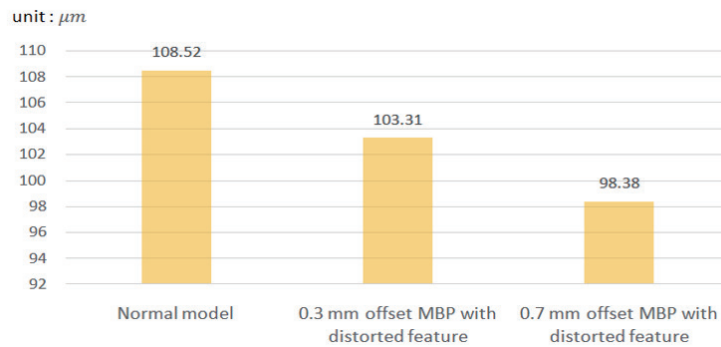Fig. 7.   (Color online) Von-Mises stress of bipolar plates in fuel cell stack model. (a) Full model and (b) bipolar plate.

unit : μm

Fig. 8. (Color online) Maximum vertical deformation values of normal MBP and MBP with distorted design feature.
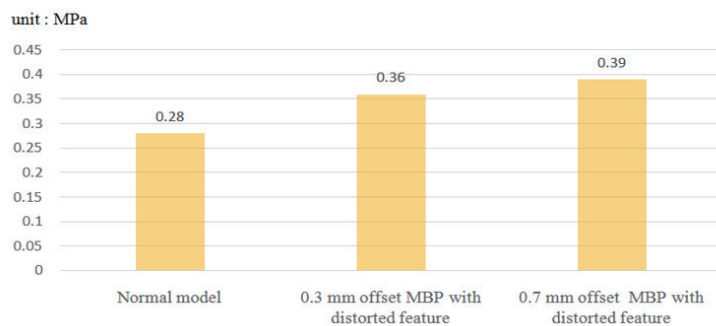
unit : MPa

Fig. 9. (Color online) Maximum vertical stress values of normal MBP and MBP with distorted design feature.

and 0.39 MPa, respectively. In comparison with the 0.3- and 0.7-mm-offset MBPs, the normal MBP model has a significantly lower vertical stress value of 0.28 MPa, representing increases of 0.08 (28.5%) and 0.11 (39.2%), respectively.

4. Discussion

The main purpose of this study is to investigate the deformation of the MBP and MEA in a fuel cell stack under the bolt clamping force.[11,26–28] Through finite element analysis, the overall deformation results of the fuel cell stack can be obtained, with the primary deformation and warping occurring in the bipolar plates. This aligns with experimental results, where the excessive deformation of bipolar plates leading to MEA extrusion damage is a common occurrence in assembled fuel cell stacks. Furthermore, the Von-Mises stress results indicate that regions with deformation in the MBP exhibit higher stress values.

If we focus on the vertical direction of stress, it is evident that there is compressive stress on the inner side of the trapezoidal bipolar plate's corner area and tensile stress on the outer side (Fig. 10). The results from the horizontal direction of stress (Fig. 11) indicate that compressive stress appears in the warped and deformed area on the MEA side of the bipolar plate, while tensile stress is observed on the flow channel side. This deformation trend in the region closely resembles the structural bending deformation in the middle area, creating a gap. This situation
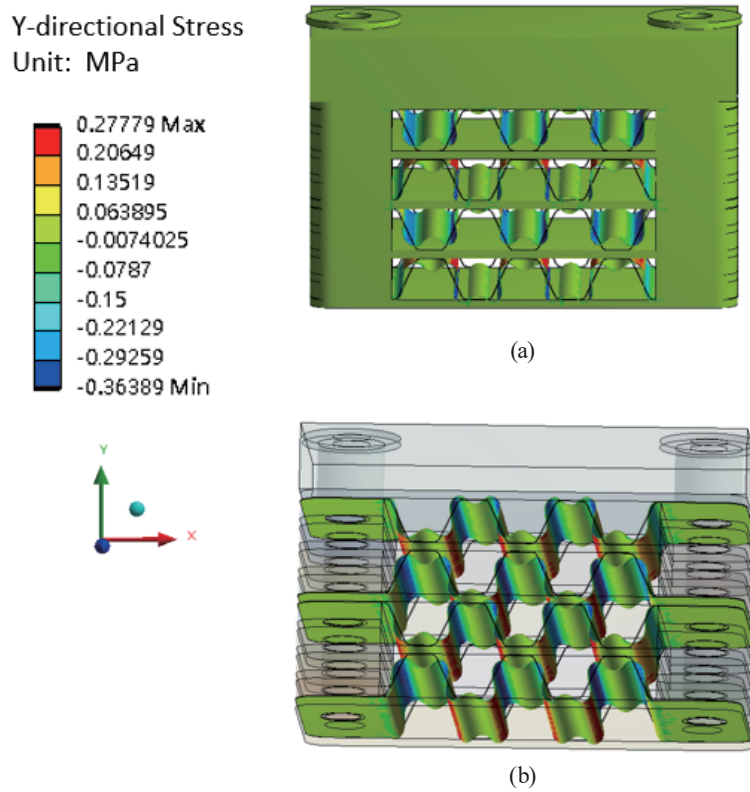
Fig. 10.   (Color online) Vertical stress of MBP. (a) Full model and (b) bipolar plate.

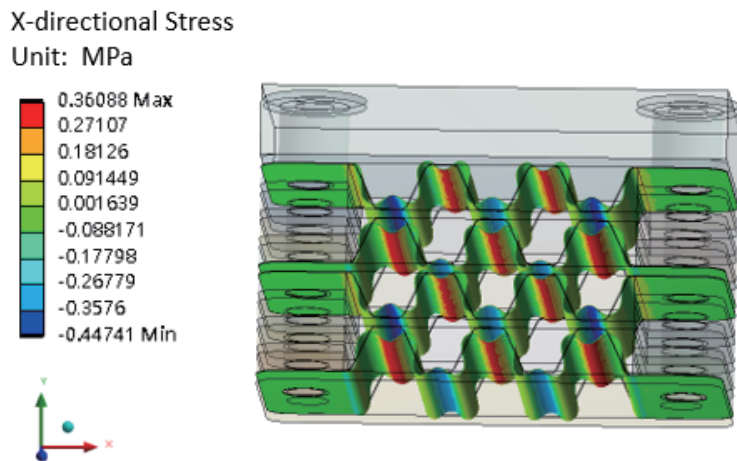Fig. 11.   (Color online) Horizontal stress of MBP.

aligns with the distribution of the gap between the MBP and the MEA interface, and this gap reduces the contact area, leading to an increase in contact resistance.

The cross-sectional deformation diagram of the bipolar plate in Fig. 12 shows that the bipolar plate with 0.7 mm deformation design characteristics can effectively reduce the vertical
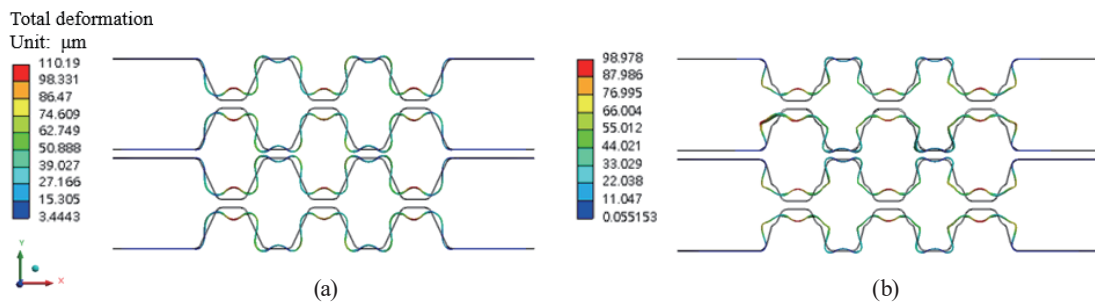
Fig. 12.   (Color online) Deformations in cross sections of (a) normal and (b) 0.7 mm distorted feature MBPs.
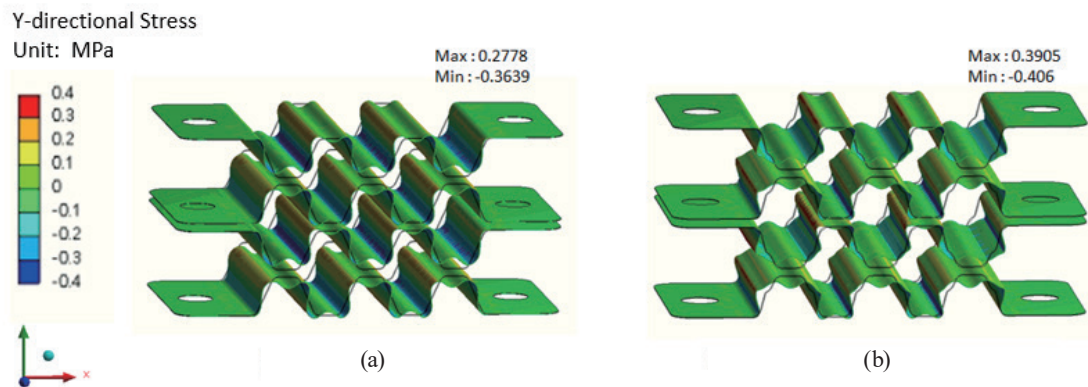

Fig. 13.   (Color online) Vertical direction stresses of (a) normal and (b) 0.7 mm distorted feature MBPs.

displacement by 10.3% compared with the general traditional bipolar plate. In this figure, the region where the bipolar plate's distortion features are increased allows for localized deformation when subjected to the force applied by bolt locking. This provision of localized permissible deformation effectively reduces the vertical warping deformation of the bipolar metal plate with the MEA.

However, the increased deformation in the region with distorted features indirectly raises the bending amount in the upper and lower turning regions of that area. Consequently, the stress in these upper and lower turning regions exhibits a noticeable increase, with the maximum stress occurring in this region. As depicted in Fig. 13, the vertical stress results for the MBP showed that the maximum stress in the upper and lower turning regions increases from the original 0.28 to 0.39 MPa. With the distorted design feature, the MBP experiences an approximately 39.2% increase in maximum stress.

5.   Conclusions

The analysis results indicate a significant impact of the assembly pressure between the MBP and the MEA in a fuel cell stack on contact resistance. Maintaining an optimal locking pressure

of the assembly bolt is essential to ensure effective contact without causing detrimental deformations. Balancing the pressure is crucial to prevent local or overall deformation, thereby preserving the gas diffusion capacity of the fuel cell stack and preventing a decrease in current density. In contrast, too little pressure can result in excessively high contact resistance. Therefore, there exists an optimal locking force for the fuel cell stack to achieve maximum efficiency.[11] Previous studies have addressed this by employing MBPs designed with distorted features, effectively improving the uneven distribution of pressure without altering the compressive force.[7,27]

In this study, special focus was placed on the interface between bipolar plates and MEA modules using contact elements for nonlinear analysis. Through these contact elements, the results of the analysis vividly illustrate the contact gap and contact pressure between the MBP and the MEA. Clear contact pressure is observed notably at the left and right edges of the contact surfaces. The interface between the MBP and the MEA primarily uses these two contact regions to transmit contact pressure and serves as the primary support for the main bending load. This situation leads to deformations on the contact surface, causing the upward or downward bending of the bipolar plate and MEA at the contact interface. The results indicate that the locking force of the bolts causes a noticeable gap between the MBP and the MEA.[29,30] This contact gap contributes to an increase in contact resistance, leading to an elevated internal resistance in proton exchange membrane fuel cells within the fuel cell stack. In this study, we simulated the deformation and warping of MBPs under clamping forces, a focus rarely seen in previous research. This approach not only considered the pressure distribution on the bipolar plates but also incorporated nonlinear contact elements to accurately simulate the contact area and pressure distribution between the MBP and the MEA, providing a more precise understanding of fuel cell performance variations. Additionally, we simulated the previous MBP design of distorted design features, comparing the effects of 0.3 and 0.7 mm misalignment gaps on plate deformation. Results showed that these design features effectively reduced the maximum vertical deformation by 10.3%, thereby increasing the contact area between the MBP and the MEA and reducing the contact resistance, significantly improving the overall fuel cell performance. Moreover, we conducted an in-depth analysis of the contact pressure distribution between the MBP and the MEA, revealing that the clamping force of the bolts led to noticeable contact gaps between the bipolar plates and the MEA. These gaps increased the contact resistance and reduced the efficiency of the cell reactions. This analytical process and its results are rare in previous studies, particularly in the comprehensive consideration of contact pressure and deformation features.

In this study, we demonstrated the potential of optimizing the MBP using distorted design features and provided specific design improvement recommendations. These results provide new insights and practical solutions for the future design and performance optimization of fuel cells. Additionally, we established an effective simulation analysis model for the deformation analysis of fuel cell bipolar plates and the analysis of contact pressure and deformation with distorted design features. In future work, we will leverage the contact pressure of MBPs with distorted design features to estimate the optimal clamping pressure and bolt parameters to maximize the efficiency of the fuel cell stack. Furthermore, we will explore altering other feature patterns of bipolar metal plates to investigate the assembly of the cell stack with minimal clamping force and to achieve optimal contact resistance.

References

1 M. Ciavarella, G. Murolo, G. Demelio, and J. Barber: J. Mech. Phys. Solids **52** (2004) 1247. https://doi.org/10.1016/j.jmps.2003.12.002

2 P. A. García-Salaberri, M. Vera, and R. Zaera: Int. J. Hydrogen Energy **36** (2011) 11856. https://doi.org/10.1016/j.ijhydene.2011.05.152

3 D. Qiu, P. Yi, L. Peng, and X. Lai: J. Fuel Cell Sci. Technol. **12** (2015) 041002.https:/doi.org/10.1016/j.ijhydene.2015.03.064

4 J. Millichamp, T. J. Mason, T. P. Neville, N. Rajalakshmi, R. Jervis, P. R. Shearing, and D. J. Brett: J. Power Sources **284** (2015) 305. https://doi.org/10.1016/j.jpowsour.2015.02.111

5 M. Ahmad, R. Harrison, J. Meredith, A. Bindel, and B. Todd: Int. J. Hydrogen Energy **42** (2017) 8109. https://doi.org/10.1016/j.ijhydene.2017.01.216.

6 S. Kandlikar, Z. Lu, T. Lin, D. Cooke, and M. Daino: J. Power Sources **194** (2009) 328. https://doi.org/10.1016/j.jpowsour.2009.05.019

7 W. Chang, J. Hwang, F. Weng, and S. Chan: J. Power Sources **166** (2007) 149. https://doi.org/10.1016/j.jpowsour.2007.01.015

8 I. Gatto, F. Urbani, G. Giacoppo, O. Barbera, and E. Passalacqua: Int. J Hydrogen Energy **36** (2011) 13043. https://doi.org/10.1016/j.ijhydene.2011.07.066

9 M. Ismail, A. Hassanpour, D. Ingham, L. Ma, and M. Pourkashanian: Fuel Cells **12** (2012) 391. https://doi.org/10.1002/fuce.201100054

10 X. Wang, Y. Song, and B. Zhang: J. Power Sources **179** (2008) 305. https://doi.org/10.1016/j.jpowsour.2007.12.055

11 V. Radhakrishnan and P. Haridoss: Int. J. Hydrogen Energy **36** (2011) 14823. https://doi.org/10.1016/j.ijhydene.2011.05.185

12 C.-Y. Wen, Y.-S. Lin, and C.-H. Lu: J. Power Sources **192** (2009) 475. https://doi.org/10.1016/j.jpowsour.2009.03.058

13 C. Carral and P. Mele: Int. J. Hydrogen Energy **39** (2014) 4516. https://doi.org/10.1016/j.ijhydene.2014.01.036

14 Y. Song, C. Zhang, C.-Y. Ling, M. Han, R.-Y. Yong, D. Sun, and J. Chen: Int. J. Hydrogen Energy **45** (2020) 29832. https://doi.org/10.1016/j.ijhydene.2019.07.231

15 S.-J. Lee, C.-D. Hsu, and C.-H. Huang: J. Power Sources **145** (2005) 353. https://doi.org/10.1016/j.jpowsour.2005.02.057

16 H.-M. Chang, C.-W. Lin, M.-H. Chang, H.-R. Shiu, W.-C. Chang, and F.-H. Tsau: J. Power Sources **196** (2011) 3773. https://doi.org/10.1016/j.jpowsour.2010.12.090

17 A. Bazylak, D. Sinton, Z.-S. Liu, and N. Djilali: J. Power Sources **163** (2007) 784. https://doi.org/10.1016/j.jpowsour.2006.09.045

18 D. Musse and D. Lee: Energy Rep. **11** (2024) 4886. https://doi.org/10.1016/j.egyr.2024.04.052

19 T. Wilberforce, Z. El Hassan, E. Ogungbemi, O. Ijaodola, F. Khatib, A. Durrant, J. Thompson, A. Baroutaji, and A. Olabi: Renewable and Sustainable Energy Reviews **111** (2019) 236. https://doi.org/10.1016/j.rser.2019.04.081

20 X. Wang, Y. Qin, S. Wu, X. Shangguan, J. Zhang, and Y. Yin: J. Power Sources **457** (2020) 228034. https://doi.org/10.1016/j.jpowsour.2020.228034

21 C.-J. Hung, W.-J. Chen, C.-A. Lin, H.-R. Shiu, and B.-H. Chen: Energies **14** (2021) 7109. https://doi.org/10.3390/en14217109

22 S. Porstmann, T. Wannemacher, and W.-G. Drossel: J. Manuf. Process. **60** (2020) 366. https://doi.org/10.1016/j.jmapro.2020.10.041

23 Y. Leng, P. Ming, D. Yang, and C. Zhang: J. Power Sources **451** (2020) 227783. https://doi.org/10.1016/j.jpowsour.2020.227783

24 F.-B. Weng, M. M. Dlamini, and C.-H. Chen: Int. J. Electrochem. Sci. **17** (2022) 22052. https://doi.org.10.20964/2022.05.53

25 Z. Cao, W. Zhu, Z. Cheng, and Z. Yang: Int. J. Hydrogen Energy **55** (2024) 1347. https://doi.org/10.1016/j.ijhydene.2023.11.156

26 G. Jing, C. Hu, Y. Qin, X. Sun, and T. Ma: Int. J. Hydrogen Energy **58** (2024) 137. https://doi.org/10.1016/j.ijhydene.2024.01.164.

27 Y. Chen, J. Zhao, C. Jin, Y. Ke, D. Li, and Z. Wang: Membranes **12** (2022) 645. https://doi.org/10.3390/membranes12070645

28 X. Q. Xing, K. W. Lum, H. J. Poh, and Y. L. Wu: J. Power Sources **195** (2010) 62. https://doi.org/10.1016/j.jpowsour.2009.06.107

29   I. Taymaz and M. Benli: Energy **35** (2010) 2134. https://doi.org/10.1016/j.energy.2010.01.032
30   H. Talebi-Ghadikolaee, M. M. Barzegari, and S. Seddighi: Int. J. Hhydrogen Energy **48** (2023) 4469. https://doi.org/10.1016/j.ijhydene.2022.10.270